Article

Micromechanical Analysis in Applications of Active Mono-Slip and Continuum Dislocations in the MDCM

Temesgen Takele Kasa [1,2]

1 Department of Mechanical Engineering, College of Electrical and Mechanical Engineering, Addis Ababa Science and Technology University, Addis Ababa P.O. Box 16417, Ethiopia; ttkh1@pukyong.ac.kr
2 Department of Mechanical Engineering, Pukyong National University, Yongdang Campus, 365, Sinseon-ro, Nam-Gu, Busan 48547, Korea

Abstract: The key purpose of this paper is to propose a mono-slip-dependent continuum dislocation method for matrix-dominated composite structure (MDCS) analysis. The methodology focuses on dissipation energy theories utilizing a continuum dislocation method (CDM) integrated with small-strain kinematics. The mathematical modeling of the CDM comprises active mono-slip system formulations, thermodynamic dislocation analysis (TDA), free energy dissipation analysis, and the progression of dislocations. Furthermore, zero and non-zero energy dissipation due to dislocation progression is formulated by using an energy minimization technique with variational calculus. The numerical analysis, performed with Wolfram Mathematica©, is presented using zero and non-zero energy dissipation energy formulations. The outcomes indicate that the formulated approach can be effective for obtaining optimal analysis results for matrix-dominated composite (MDC) materials with a mono-slip system. In sum, this study confirms the feasibility of using the proposed approach to investigate MDCS with inclusions.

Keywords: mono-slip; MDCS; CDM; distortion; active slip; TDA; MDC

1. Introduction

Composite materials are used as structural elements in a wide variety of applications, including space shuttles, marine vehicles, automobiles, and construction sectors. These materials are widely applied for their remarkable in-plane stiffness, bending stiffness, ultimate strength, light weight, and good thermal expansion coefficient during deformation [1–4]. In a matrix-dominated composite structure (MDCS), permanent deformation can be expressed by the limit of dislocation nucleation and the dislocation energy [5]. The nucleation and energy of the dislocation create internal structural irregularities. These internal irregularities in a matrix-dominated composite (MDC) structural arrangement have been analyzed in the context of intermittent crystallographic dislocations. This means that the created nucleation of dislocations can be grouped to reduce the energy dissipation of the crystals. The new initiation of dislocation is principally the result of the dissipation of crystal energy. Therefore, the initiation of dislocation in the MCDS activates the dislocation energy. Hence, the dislocation energy impedes plastic flow through the dissipation of crystal energy. Thus, all microstructural analyses related to permanent deformation should follow the rules of thermodynamics [6]. This can be a practical method to study MCDS related to poly-dimensional dislocation propagation. Furthermore, experimental investigations have indicated that dislocations in a strained crystal do not act in a fully random arrangement. Along with the above limitation, the distorted MDCS does not have a consistent dislocation density from one end to the other in the inner structure of the unit cell [7–12].

Therefore, in a micromechanical approach, discrete dislocation analysis is not sufficient to describe the individual and/or small number of dislocations in MDCS. This method has difficulty defining strains along the dislocation line inside the dislocation core [13–17]. In

contrast to the micromechanical method, the typical characteristics of materials at the macro level can be accurately investigated through the continuum principle. With this concept in mind, the continuum mechanics approach, which aims to include the size effect of the dislocation flow through a strain gradient (nonlocal) component by combining classical and local representations, is based on a massive number of continuous dislocations [18–22]. Accordingly, there is a huge gap between the micro- and macroscales. Bridging the two extremes requires an appropriate meso-model, namely, continuum dislocation formulations. The formulations of continuum dislocation include the length scale of the material, and hence, the size effects can be accounted for in the mesoscale model [23–27]. The length scale of the material in a deformed body becomes substantial in the mechanics of the material. This raises a significant question, namely, the degree to which the overall macro-level mechanical properties (strength, hardness, etc.) are determined by the collective parametric length scale associated with the distinctive microstructural magnitude of the material [18,28–31].

In this study, we performed an analysis of free energy in unit cells (UCs) that were subjected to dislocation in an active mono-slip system. In the proposed approach, energy is incorporated into the structure caused by geometrically necessary dislocations (GNDs) to determine the material parametric length [6,32–34]. The composite material is assumed to comprise a bi-periodic array of unit cells. Additionally, the unit cell is directly isotropic, and the matrix domination is higher, contains free inclusions without dislocation, and is exposed to normal shear stress through kinematic boundary conditions. Many theories in micromechanical analysis use a higher-order PDE approach. This method can be physically applied to the analysis of energy in the material structure, the linear increase in the microstructural energy, and the standardized value of the density of dislocation (DOD). However, the energy increases to infinity as the DOD approaches a certain critical saturation stage [29,35,36]. Saturated forms of DOD have constant material parametric values and do not allow for the dense packing of trapped dislocation potential; these outcomes are due to the discrete characteristics of the unit cell. Thus, the energy in the proposed formulation has an internal length scale to provide a macroscopically apparent size.

Collectively, the above-mentioned works present the benefits and weaknesses of different methods of MDCM. From the above review, we observed that there is a substantial gap in the understanding of derivations of continuum dislocation constituents, such as slip formulations, thermodynamic relationships, free energy determinations, threshold values, and the evolution of dislocation. In this regard, our study plays a key role in filling the gap in matrix-dominated composite structure analysis using variational calculus.

The key aim of this work is to propose a simple approach based on continuum dislocation theory to analyze the plastic phenomenon of MDCM exposed to shear. Derivations of the continuum dislocation components, including slip formulation, thermodynamic relationships, free energy analysis, threshold values, and the progression of dislocation, are described. In general, dissipation energy is analyzed. Furthermore, the non-dissipation forms of the equations are evaluated using variational calculus. The energy minimization method is applied to the above two formulations. Finally, the capability of the proposed approach is demonstrated through the homogenization principle with constituents that exhibit different mechanical behaviors.

2. Continuum Dislocation Formulation

2.1. Kinematics

Figure 1 shows the simplest representation of the MDCS unit cell to simplify the analytical formulations. The arrangement in Figure 1 is the Cartesian coordinate system, with $x = (x_1, x_2, x_3)$ and $y = (y_1, y_2, y_3)$, where x_i denotes the local system of coordinates to define the microscopic unit cell, and y_i represents the global coordinates to designate the unit cell. For a unit cell with a size of $2\xi_i$ and $2w_i$, we select the micro-coordinates x_i defined by $x_i(2\xi_i, 2w_i)$. The 2D MDCS comprises rectangular elastic inclusions in a

plastically deformed matrix. The inclusions can be established in a bi-hexagonal periodic array, as presented in Figure 1.
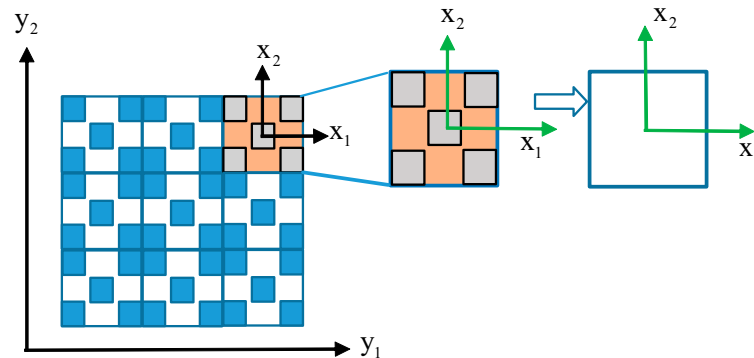
Figure 1. 2D simplest representation of the MDCS unit cell.

Cleveringa et al. [28,29] analyzed MDCS by applying discrete dislocation to validate the precision of the modern continuum dislocation concept in reproducing size-dependent outcomes. Two forms of inclusion are considered, which have an identical fractional area of 0.2 but dissimilar geometrical arrangements of the strengthening material phase. The main materials are square geometrical inclusions segmented by the matrix, and the inclusions are rectangular and separated by matrix materials. As a consequence of the discontinuous structure of the unit cells, the analysis can be implemented discretely, in which the width is represented by *2w* and the height is represented by $2\xi\left(w/\xi = \sqrt{3}\right)$, as illustrated in Figure 2. The inclusions have a size of $2w_f \times 2\xi_f$, with $\xi_f = w_f = 0.416\xi$ for square geometry and $\xi_f = 2w_f = 0.588\xi$ for quadrangular geometry. Shearing occurs in the x_1-direction; thus, boundary conditions (BCs) can be formulated as follows:

$$u_1(t) = \pm\xi\Gamma, \; u_2(t) = 0 \; along \; x_2 = \pm\xi \tag{1}$$

where $\Gamma(t)$ denotes the shear strain as a function of time.
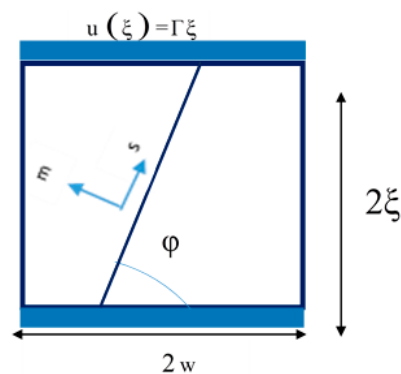
Figure 2. Active mono-slip system with a unit cell (UC) of ξ thickness.

2.2. Mono-Slip Analysis in the Continuum Formulation

Here, we show that the lateral boundary condition in the free form can be investigated analytically. Additionally, clamped micro-BCs of the top and bottom sections of the unit cell can be formulated using the standard analytical model, where, based on the principle of plasticity, the overall displacement field in the gradient **u** signifies the total displacement field in a compatible formulation. The dislocation loop is singular and positioned on the single-slip plane, and the Burgers vector points in the right direction toward the path of the

slip. Based on the above concept, the inverse plastic distortion on the loop is formulated as Equation (2).

$$- Y_{ij} = b_i n_j \delta(s) \tag{2}$$

where b_i denotes the Burgers vector, δS is the cut surface lying on the slip plane, and n_j is the vector perpendicular to the plane of the slip.

This inverse plastic distortion describes the creation of dislocation by cutting a perfect crystal along the surface S and shifting the structure beneath this surface by one Burgers vector [37]. In general, the summation of the reversible and irreversible distortion fields contributes to the total distortion result:

$$Y = Y^e + Y^p \tag{3}$$

where Y^e and Y^p describe the reversible and irreversible distortions in the material system. Due to the existence of boundary lines between dislocations, the incompatibly of the two phases are represented by the GND [38]. A huge number of loops pass through the slip planes, and the average distance between them is considerably smaller than the material characteristic scale size of the standard piece; we go one step further and propose a unique formulation for the plastic distortions created by this slip system, expressed as

$$Y_{ij} = Y(x)s_i m_j \tag{4}$$

where m represents a normal vector that points toward the slip direction, and s denotes the slip path. The analytical analysis fundamentally depends on the continuum dislocation principle of unit cell plasticity owing to particular situations in which shape variations are insignificant and the response of the material is rate independent [39]. The governing equations can be abridged by employing tensor analysis in a coordinate system. The plastic strain, represented by ε_{ij}^p, and plastic rotations, designated by Ω_{ij}, are the symmetric and anti-symmetric parts of the irreversible deformations:

$$\varepsilon_{ij}^p = \left(Y_{ij} + Y_{ji} \right)/2, \quad \Omega_{ij} = \left(Y_{ij} - Y_{ji} \right)/2 \tag{5}$$

The strains in the reversible phase can be estimated as the differences between the overall incompatible strains and the irreversible strain state. Then, the reversible strain tensors are

$$\varepsilon_{ij}^e = 1/2\left(u_{ij} + u_{ji} \right) - \varepsilon_{ij}^p \tag{6}$$

The fundamentals of the continuum dislocation principle of unit cell plasticity applied in this work are supported by Fleck, whose described the concept of lattice incompatibility [40]. The plastic distortion field Y^e can be obtained by the sum of its symmetric strain and anti-symmetric rotation fields,

$$Y^e = \varepsilon^e + \Omega^e \tag{7}$$

where ε^e denotes elastic strain and Ω^e is the reversible torsional strain. We assumed that the elasticity is linear, disregarding the 'shape nonlinearity' portion. The fundamental concept of the elastic deformation of the UC is not harmonious with regular distortion, which is obtained through a continuously differentiable displacement component. However, reversible distortion is sufficient to represent geometrically necessary dislocations [8]. In this framework, the number of dislocations/unit area can be described as

$$\rho = 1/b \left| \varepsilon_{ijkl} Y_{,k} m_l n_j \right| \tag{8}$$

where ρ denotes the number of dislocations/unit area. In this model, the theory addressing the incompatibility of the distortion is incorporated into the constitutive formulation through the influence of strain hardening. Meanwhile, the lattice incompatibility can be described by a gradient of the reversible or irreversible distortion field, and the material

parametric length scale analysis can be performed on the basis of the one-dimensional principle. Through the above concepts, a natural evaluation of incompatibility can be investigated with the Nye dislocation density principle [32]. Nye presented an imperative characteristic of dislocations, so the dislocation density tensor is represented by

$$\alpha_{ij} = \varepsilon_{jkl} Y_{il,k} \tag{9}$$

An unavoidable tensor α_{ij} indicates the presence of GND. The dislocation in the unilateral loop is named the density of dislocation (DOD), in which the geometrical meaning of the tensor is denoted by a random microscopic outer unit normal vector (**da**) and $\boldsymbol{\tau}$, the tangent to the dislocation line passing over the surface, so the Burgers vector is expressed as

$$b = Y_{ij} n_j da \tag{10}$$

Equation (10) can be used to calculate the total number of dislocations in the same direction. Therefore, the net Burgers vector **b** in any section is constrained by a locked graph. On the basis of the continuum dislocation principle, we can deduce the magnitude from the Burgers vector in the form of resultants for overall dislocations that cross the surface **da**. Therefore, in the deformation of the mono-slip MDCS, the dislocation density is described as follows:

$$\alpha_{ij} n_j = p_i \varepsilon_{jkl} Y_{,k} m_l n_j \tag{11}$$

In this work, an active mono-slip in the unit cell is assumed in the analysis of the state of the in-plane strain. The fields of the strain tensors are (refer to Figure 2)

$$\varepsilon_{11} = 0, \varepsilon_{12} = \varepsilon_{21} = \frac{1}{2} u_{1,2}, \varepsilon_{22} = u_{2,2} \tag{12}$$

Accordingly, the resultant Burgers vector of the overall lines of dislocation intersects with the area and is normal to the x_3-axis, and it is also in the same direction as the slip **s** and the scalar dislocation density. If the shear strain is necessarily small, then the unit cell elastically deforms with the following displacement:

$$u_1 = \Gamma x_2, \ u_2 = 0 \tag{13}$$

We can use the direction of slips that are normal to the x_3-axis and tilted with a given angle away from the x_2-axis. The lines of dislocation are in the same direction as the x_3-axis. An active single-slip system of distortion in the plastic state is given by

$$Y_{ij} = Y s_i m_j \tag{14a}$$

where $s = (\cos \varphi, \sin \varphi, 0)$ denotes the slip direction, and $m = (-\sin \varphi, \cos \varphi, 0)$ represents the vector that is normal to the mono-slip. As Y depends only on x_2, there can be two branches of the dislocation density tensor for Nye's formulation, specifically, $\alpha_{13} = Y_{,2} \cos \varphi \sin \varphi$ and $\alpha_{23} = Y_{,2} \sin^2 \varphi$. We assume that Y depends only on $x_2 : Y = Y(x_2)$. Due to the given boundary, the dislocation is prevented from passing $x_2 = 0$ and $x_2 = \xi$. Therefore,

$$Y(0) = Y(\xi) = 0 \tag{14b}$$

2.3. Thermodynamic Principles

To formulate the MDCS in Figure 1, we can apply free energy theory to investigate the UCs with the required accuracy. This postulation suggests that we can acquire identical nominal material properties since an ideal unrestrained and free MDCS uses identical microstructures for the loaded and constrained unit cells. Hereafter, we can perform the micromechanical calculations since a composite material is composed of a vast number

of UCs. For a reversible and tough material, the total amount of energy is the same as the time derivative of free energy plus the power stored in all of the UCs, which is

$$\prod = \frac{d}{dt} \int_R \Theta(\varepsilon_{ij}, Y_{ij}, \alpha_{ij}) dx + \Phi \leq 0 \tag{15}$$

The required extent of power in any solid material can be measured from the scheme of energy. For this study, the power is formulated as

$$\Phi = \int_{\partial Y} \left(\sigma_{ij} n_j \dot{u}_i + \sigma_{ijk} n_k \dot{Y}_{ij} \right) da \tag{16}$$

where Φ is the accumulated power, and σ represents stress. We infer that the stresses expressed in terms of higher-order calculus are included under this theory because the gradient of irreversible distortion is based on the density of the stored energy. Thus, we can transform the surface integral into a volume integral by Gauss's principle, and the mathematical requirement can be satisfied for an arbitrary R. At this juncture, the combination of the first and second principles of thermodynamics can be defined by

$$\zeta_{ij} \dot{u}_{ij} + \lambda_{ij} Y_{ij} + \zeta_{ijk} \dot{Y}_{ij,k} \geq 0 \tag{17}$$

This confirms that ζ_{ij} and ζ_{ijk} denote the normal and higher-order stresses, respectively, which cause energy dissipation through the heating of the crystal. Tensor λ_{ij} describes a non-uniform flow of heat; it assumes the same meaning as in the frictional stress formula. Thus, λ_{ij} and ζ_{ijk} denote the heat caused by homogeneous and inhomogeneous irreversible distortions, respectively.

$$\mathbb{Q} = \mathbb{Q} \left(\dot{u}_{ij}, \dot{Y}_{ij}, \dot{Y}_{ij,k} \right) \tag{18}$$

The tensors described as ζ_{ij}, λ_{ij} and ζ_{ijk} for irreversible progressions are related to $\dot{u}_{ij}$, Y_{ij} and $\dot{Y}_{ij,k}$ and described by the next formulation.

$$\zeta_{ij} = \mathbb{Q}_{,\dot{u}_{ij}}, \lambda_{ij} = \mathbb{Q}_{,\dot{Y}_{ij}}, \zeta_{ijk} = \mathbb{Q}_{,\dot{Y}_{ij,k}} \tag{19}$$

Consequently, each model of continuum dislocations can be formulated by the two energy functions, namely, free energy and potentials of dissipation. In the isothermal formulation, we require the free energy density to be contingent on the elastic state ε_{ij}^e. The free energy in terms of ε_{ij}, Y_{ij} & α_{ij} is given as follows:

$$\Theta(\varepsilon_{ij}, Y_{ij}, \alpha_{ij}) = \frac{1}{2} \Re_{ijkl} \varepsilon_{ij}^e \varepsilon_{kl}^e + \Theta_m(\alpha_{ij}) \tag{20}$$

where $\Theta_m(\alpha_{ij})$ denotes the energy of the dislocation network of the system. When ρ increases, there must be some threshold value, ρ_s, after which new dislocation structures grow, including sub-grains and cell structures or new grain boundaries. Hence, additional parameters must come into play. If we preclude the networked structure of dislocation from surfacing, the dislocation network energy approaches infinity as $\rho \rightarrow \rho_s$ [41]. Then, the dislocation network energy $\Theta_m(\alpha_{ij})$ for the UC distortion in the active mono-slip system can be evaluated as follows:

$$\Theta_m = K * G_{12} * \ln(1 - \rho/\rho_s)^{-1} \tag{21a}$$

where K denotes a material constant, G_{12} represents the modulus of shear, b is the Burgers vector, and ρ_s denotes the saturated dislocation density (SDD). The GND energy components imply two important details. First, the network of dislocation energy is directly proportional to the DOD when the dislocation is small. Second, the existing SDD, which

indicates the nearby grouping of dislocation, can have identical signs to those of the newly created permissible dislocation in the unit cell. Assuming that the material is isotropic and contains inclusions, for simplicity, the elastic behavior of the unit cell in both the matrix and fiber materials is considered isotropic [18]. The modulus of elasticity of the matrix can be formulated as

$$\Re = 2G_{12}\left(I' - \frac{\nu}{1-2\nu}I \otimes I\right) \tag{21b}$$

where G_{12} is the shear modulus, ν is Poisson's ratio, I represents a quadratic-order identity tensor, and I′ denotes a polynomial-order identity tensor. This is also true for the fiber, but the shear modulus changes to G_{12}^*. The GND term [41] ensures a direct increase in energy from a low density of dislocation (ρ). Then, energy approaches infinity as the density of dislocation reaches the saturated level, symbolized as (ρ_s). Therefore, an energetic barrier is provided to prevent over-saturation. For the dissipation potential, numerous models can be considered. The simplest model assumes that the dissipation is zero. In this case, all tensors (ζ_{ij}, λ_{ij} and ζ_{ijk}) vanish, and the functions u_{ij} and Y_{ij} can be found from energy minimization. From the above point of view, the total energy functional is represented by the following:

$$\prod[u_1, u_2, Y] = wL\left\langle \begin{array}{c} \frac{1}{2}\Re(u_{2,2})^2 + \frac{1}{2}G_{12}(u_{1,2} - Y\cos 2\varphi)^2 + \frac{1}{4}G_{12}Y^2\sin^2 2\varphi \\ +G_{12}\left(u_{2,2} - \frac{1}{2}Y\sin 2\varphi\right)^2 + G_{12}k*\ln\left(1 - \frac{|Y_{,y}||\sin\varphi|}{b\rho}\right)^{-1} \end{array} \right\rangle_{a=\xi} \tag{21c}$$

where $\langle\bullet\rangle = \int_0^a \bullet\, dx_2$.

Based on the continuum dislocations, the main constitutive and balance equation is defined as a basic formula for the active mono-slip equation. The first visco-plastic framework can be translated into a purely elastoplastic context, for which analytical equations can be determined through the shear analysis. The displacement field in a unit cell and the mean shear distortions can be measured by the continuum dislocation approach. To evaluate this displacement, the function of the overall energy is simplified so that it depends on a functional $Y(x_2)$ only. First, the function $Y(x_2)$ is defined, and then variational calculus is applied to Equation (21a) with respect to u_1 and u_2 to determine the strain in the analysis of shear (shear strain) deformation.

$$\left\{ \begin{array}{c} u_{1,22} = Y_{,2}\cos 2\varphi \\ \Re u_{2,22} + 2G_{12}u_{2,22} = G_{12}Y_{,2}\sin 2\varphi \end{array} \right\} \tag{21d}$$

As previously stated, using Equation (22a) as a boundary condition, we can apply simple integration to Equation (21a) to formulate the displacement fields and shear strain. Then, we can obtain a general equation for the continuum approach to describe the analogous shear strain component in the defined boundary conditions [42].

$$Y(0) = Y(\xi) = 0 \tag{22a}$$

Subsequently, we can apply terms to divide the displacement into **u₁** and **u₂** components. The effect of the two components of displacement results in shear strain on the unit cell and a mesoscopic internal parametric length created from the overall heterogeneous internal strain component. Thus, in a small-strain calculation, the two displacement components can be directly derived because the small-strain equation is linear. In the unit cell, the mesoscopic internal parametric length of shear strain can be stated in terms of the DOD pattern. The shear strain varies with a length scale equal to the DOD formulation, designated by α_{ij}. Integrating (22) and using the boundary conditions (22a) results in the following equation:

$$\left\{ \begin{array}{c} u_{1,2} = \Gamma + Y\cos 2\varphi - Y^{ave}\cos 2\varphi \\ u_{2,2} = Yk\cos 2\varphi - kY^{ave}\cos 2\varphi \end{array} \right\} \tag{22b}$$

where $K = G_{12}/\Re + 2G_{12}$, and $Y^{ave} = \frac{1}{\xi}\int_0^{\xi} \bullet dx_2$. By substituting (22b) into (21a), we can minimize the functional formulation in the form of a distortion variable (Y).

$$\prod[Y] = wL\left\langle G_{12}\left(\begin{array}{c} \frac{1}{2}Y^2\sin^2 2\varphi - \frac{1}{2}\kappa Y^2\sin^2 2\varphi + \frac{1}{2}\kappa(Y^{ave})^2\sin^2 2\varphi \\ +\frac{1}{2}(\Gamma - Y^{ave}\cos 2\varphi)^2 + k\left(|Y_{,2}||\sin\varphi|(b\rho)^{-1} + \frac{1}{2}\left(Y_{,2}\sin\varphi(b\rho)^{-1}\right)^2\right) \end{array} \right)\right\rangle_{a=\xi} \tag{22c}$$

The last part of (21a) that contains the dislocation density variable can be simplified:

$$\ln\left(1 - \frac{|Y_{,2}||\sin\varphi|}{b\rho}\right)^{-1} = |Y_{,2}||\sin\varphi|(b\rho)^{-1} + \frac{1}{2}\left(Y_{,2}\sin\varphi(b\rho)^{-1}\right)^2 \tag{22d}$$

2.3.1. Zero Energy Dissipation Case

In this work, the energy dissipation rate increases when minimizing the volume fraction of the fiber and its modulus. The approach that minimizes the volume fraction increases the dissipation energy to the maximum level. For complete slip, the increase in dissipation energy is directly proportional to the change in shear stress. The formulation for active mono-slip is based on the flow rule; thus, the dissipation potential is described as

$$\mathbb{Q} = K\left|\dot{Y}\right| \tag{23}$$

In the zero-resistance case, the formulation of plastic strain requires the simplification of the overall energy. Subsequently, U will be graphically convex with respect to Y and $Y_{,2}$ in the variational formulation, which should provide accurate results [33].

Formulations

To simplify the energy functional equation, some dimensionless quantities are introduced. Continuum dislocation formulations in a single-slip mechanism require a crucial formula that includes the balance and the evolution. Both have a common type of material, geometry, and parametric length. We aimed to develop an analytical model that shows distinctive features of the theory, independent of a specific selection of material parameters. Similarly, we performed a dimensionless analysis on the two components to explore how definite integrations of the parameters affect the outcome predicted by this method. The dimensionless variables include the elevation of the UC, which can be considered comparable to a domain elevation described by $\overline{x}_2$ and is denoted by w. The newly introduced variable $\overline{x}_2$ varies in the range $(0, \overline{\xi})$. By using the newly introduced variables, the energy functional is formulated as follows:

$$E = b\rho_s\prod(wLG_{12})^{-1}, \overline{x}_2 = x_2 b\rho_s, \overline{\xi} = \xi b\rho_s \tag{24}$$

The energy functional equation expands into the following formula:

$$E[Y] = \left\langle \begin{array}{c} \frac{1}{2}Y^2\sin^2 2\varphi - \frac{1}{2}\kappa Y^2\sin^2 2\varphi + \frac{1}{2}\kappa(Y^{ave})^2\sin^2 2\varphi \\ +\frac{1}{2}(\Gamma - Y^{ave}\cos 2\varphi)^2 + k|Y'||\sin\varphi| + \frac{1}{2}Y'^2\sin^2\varphi \end{array} \right\rangle_{a=\xi} \tag{25}$$

In Equation (25), the differentiation is performed with respect to $\overline{x}_2$, and for simplicity, the bars over x_2 and ξ are removed. To determine the threshold value, Equation (25) is minimized by incorporating the following boundary conditions:

$$Y(0) = Y(\xi) = 0 \tag{26}$$

A threshold value exists in the variational problem of (25) when the shear strain is less than a set value; in this case, there is no dislocation nucleation, which implies that the value of the plastic shear strain is equal to zero. Near the initial value of plasticity, the density of

dislocation should be small, so we can remove the last term of the equation. Moreover, the boundary layer width approaches zero as the plastic shear strain tends toward a threshold value. This provides the key to obtaining the value of the threshold through the minimizing sequence of Equation (27):

$$Y = \left\{ \begin{array}{l} \frac{Y_m x_2}{\varepsilon} \ for \ x_2 \in (0, \varepsilon), Y_m \ for \ x_2 \in (\varepsilon, \xi - \varepsilon), \\ \frac{Y_m}{\varepsilon}(\xi - x_2) \ for \ x_2 \in (\xi - \varepsilon, \xi) \end{array} \right\} \tag{27}$$

where Y_m is a constant value, and ϵ is a new infinite length that moves toward zero as the plastic shear strain tends toward a threshold value. Substituting (27) into the energy functional (25) by removing the last term and ignoring small terms of order ϵ and higher results in the following expression of the energy functional:

$$E[Y_m] = \frac{1}{2}\xi\left[\Gamma^2 - 2\Gamma Y_m \cos 2\varphi + Y_m^2 \cos^2 2\varphi + Y^2 \sin^2 2\varphi\right] + 2k|Y||\sin \varphi| \tag{28}$$

Simple analysis shows that to achieve a minimum value in (28), the minimized plastic distortion is different from zero if, and only if,

$$\Gamma > \Gamma_{en} = 2k|\sin \varphi|\left(\xi\left|1 - 2\sin^2 2\varphi\right|\right)^{-1} \tag{29a}$$

Dislocations are not nucleated when deformation achieves. $Y_m = 0$. Recall that the sign of Y_m relies on the inclination of φ. Therefore, the angle φ is positive if $0^0 \le \varphi \le \pi/4$ and negative if $\pi/4 \le \varphi \le \pi/2$. With the size effect of the original length expressed in terms of ξ, the energy threshold value can be formulated as

$$\Gamma_{en} = 2k|\sin \varphi|\left(\xi b\rho_s\left|1 - 2\sin^2 2\varphi\right|\right)^{-1} \tag{29b}$$

The threshold value deviates from the well-known Hall–Petch relationship. The term can be explained by the following condition: the deviation in (26) is through slip fields, which does not allow dislocations to penetrate grain boundaries. Boundary conditions in the grain boundaries cause Y' to change its direction in the range $(0, \xi)$. In 1-D dislocation theory, the analysis of the previous formulations suggests that the minimizer can be found from the following:

$$Y = \left\{ \begin{array}{l} Y_1 x_2 \ for \ x_2 \in (0, \ell), Y_m \ for \ x_2 \in (\ell, \xi - \ell), \\ Y_1(\xi - x_2) \ for \ x_2 \in (\xi - \ell, \xi) \end{array} \right\} \tag{30}$$

where Y_m is a constant value, and ℓ is an unknown parametric length, with $0 \le \ell \le \xi/2$ and $Y_1(\ell) = Y_m$. The total energy functional is

$$\begin{aligned} E = 2&\left\langle \frac{1}{2}Y_1^2 \sin^2 2\varphi - \frac{1}{2}kY_1^2 \sin^2 2\varphi + k|Y_{,2}||\sin \varphi| + \frac{1}{2}Y'^2 \sin^2 \varphi \right\rangle + \frac{1}{2}Y_1^2 \sin^2 2\varphi(h - 2l) - \frac{1}{2}kY_1^2 \sin^2 2\varphi(h - 2l) \\ &+ \frac{1}{2}h\left[kY^{ave} \sin^2 2\varphi + \Gamma^2 - 2\Gamma Y^{ave} \cos 2\varphi + (Y^{ave})^2 \cos^2 2\varphi\right] \end{aligned} \tag{31}$$

$$Where \ \langle \bullet \rangle = \int\limits_0^l \bullet \ dx_2$$

From the above analysis, we obtained the optimal method to begin averaging the appropriate variable of plastic distortion, aiming to define other variables to examine the evolution of dislocations and other plasticity-related factors. More importantly, we discovered that the average plastic distortion equation strongly suggests the micro-level

kinematics in the averaging formulas, which should be a physically realistic representation of the incorporated length scale.

$$Y^{ave} = \frac{1}{\xi} 2 \left(\int_0^\ell Y_1 dx_2 + (\xi - 2\ell) Y_m \right) \tag{32}$$

To generalize the concept, we can vary the energy function Equation (31) Y_1. Then, we can perform integration by parts:

$$Y^{ave} \cos^2 2\varphi + kY^{ave} \sin^2 2\varphi + Y_l \sin^2 2\varphi - kY_l \sin^2 2\varphi = kY_1'' \sin^2 \varphi + \Gamma \cos 2\varphi \tag{33a}$$

To simplify our modeling, it is better to subject $Y_1(y)$ to boundary conditions:

$$Y_1(0) = 0, Y_1(\xi) = Y_m \tag{33b}$$

Next, (31) is manipulated using variation with respect to ℓ, which establishes an additional boundary condition.

$$y = \ell, Y_{1,2}(\ell) = 0 \tag{33c}$$

We can also use the variation formulation again on the energy functional Equation (33) with respect to Y_m, followed by integration by parts to simplify it.

$$2k|signY_1'||\sin\varphi| + Y^{ave}\cos^2 2\varphi + \kappa Y^{ave} \sin^2 2\varphi = \Gamma \cos 2\varphi - Y_m \sin^2 2\varphi + kY_m \sin^2 2\varphi(h - 2l) \tag{34}$$

The generation of the described evolution equation is based mainly on an energy minimization formula in the zero-energy dissipation case. The microstructural evolution equations introduce two modeling functions: the average distortion and the average parametric length of the material for a dislocation density. First, by assigning symbols to several components of the equation, we can reduce Equation (33) as follows:

$$\left\{ \begin{array}{l} \omega_1 = k\sin^2\varphi, \\ \omega_2 = (1-k)\sin^2 2\varphi, \\ \omega_3 = -Y^{ave}(\cos^2 2\varphi + \kappa \sin^2 2\varphi) + \Gamma \cos 2\varphi \end{array} \right\} \tag{35a}$$

Then, variational Equation (33) can be rewritten as shown below:

$$-\omega_1 Y_{l,x_2 x_2} + \omega_2 Y_l = \omega_3 \tag{35b}$$

From the above reduced variational Equation (35b), it is possible to find the characteristic equation as follows:

$$-\omega_1 r^2 + \omega_2 = 0, \ r = 2\sqrt{(1-\kappa)(\kappa)^{-1}} \cos\varphi = \pm\eta \tag{35c}$$

Therefore, the homogeneous formula in the general equation reads

$$Y_1^{cf} = A\cosh\eta x_2 + B\sinh\eta x_2 \tag{35d}$$

After that, by using Equation (35c), we search for the specific equation in the heterogeneous formula in the following form:

$$Y_{1p} = \omega y + D \tag{35e}$$

By inserting Equation (35e) into the differential equation, we obtain the following formula:

$$\omega_2 \omega y + \omega D = \omega_3 \tag{35f}$$

This implies that $\omega = 0$, $D = \omega_3/\omega_2$. Based on this principle and using Equation (33) with the boundary conditions (33a), the following equations are formulated.

$$Y_{1p} = \left(\Gamma \cos 2\varphi - Y^{ave} \cos^2 2\varphi - \kappa * Y^{ave} \sin^2 2\varphi\right)\left[(1 - \kappa)\sin^2 2\varphi\right]^{-1} \tag{35g}$$

The result of the differential formula (35b) is the summation of Equations (35d,g), formulated as Equation (35h):

$$Y_1 = Y_1^{cf} + Y_{1p} = A\cosh\eta x_2 + B\sinh\eta x_2 + Y_{1p} \tag{35h}$$

The constants A and B in Equation (35h) can be derived from Equation (33a), and the constant A is calculated as follows:

$$A = -Y_{1p} \tag{35i}$$

For the second condition $Y_1'(0) = 0$,

$$B = -ATanh\eta\ell \tag{35j}$$

Using Equation (35i,j), Equation (35h) is finalized as shown in Equation (35k):

$$Y_1 = Y_{1p}(1 - \cosh(\eta x_2) * (1 + Tanh(\eta l) * \sinh(\eta x_2))) \quad 0 \le x_2 \le l \tag{35k}$$

In a discrete dislocation, the size effect is mostly observed in the original material flow strength. The dependence of the hardening rate on the UC size should be less pronounced than the predicted height in the continuum dislocation theory. The size influence can be enhanced through the existence of the defined boundary conditions of GNDs, which results in a fully defined interchange between the boundary layer height and the gradient of the internal irreversible strain accumulated in the bulk form. Therefore, to determine the parametric size, we expand the average distortion Equation (32). Using Equations (32), (33), (35a,b), the average of Y is expanded into the following form:

$$N = 2\left(\frac{l\eta - Tanh(\eta l)}{\eta}\right) + \frac{Cosh(\eta l) - 1}{Cosh(\eta l)}(\xi - 2l) \tag{36a}$$

$$Y^{ave} = \Gamma\cos 2\varphi \times N * \left[\xi(l - h)\cos^2 2\varphi + \left(\kappa\cos^2 2\varphi + \left(\kappa\sin^2 2\varphi + \cos^2 2\varphi\right)\right) \times N\right]^{-1} \tag{36b}$$

$$Y_m = \left(\Gamma\cos 2\varphi - Y^{ave}\left(\kappa \times \sin^2 2\varphi + \cos^2 2\varphi\right)Cosh(\eta l) - 1\right) * \left[\sin^2 2\varphi Cosh(\eta l) - \kappa\sin^2 2\varphi Cosh(\eta l)\right]^{-1} \tag{36c}$$

$$Y = (\xi \times \Gamma \times \eta(-1 + 3\cosh[l\eta] - \cosh[(l - x_2)\eta] - \cosh[(-\xi + l + x_2)\eta]\cos 2\varphi)) * \\ \left[\frac{1}{\sin^2 2\varphi}\xi \times \eta \times \cosh[l\eta] - \left(\kappa + \frac{\cos^2 2\varphi}{\sin^2 2\varphi}\right)\tanh[\xi\eta/2]\right]^{-1} \tag{36d}$$

Finally, we can calculate the parametric length from the following functional equation. The substitution of Equation (34) into (35b) yields the following equation to determine l:

$$2K|\sin\varphi|signY_1' = \left(\Gamma\cos 2\varphi - Y^{ave}\left(\kappa \sin^2 2\varphi + \cos^2 2\varphi\right)(\xi - 2l)\right) * [\cosh(\eta l)]^{-1} \tag{36e}$$

All material parameters used in this numerical analysis are well-known for the aluminum matrix. We selected these supplementary parameters for a representative mixture of discrete dislocation and continuum dislocation theory with respect to the yield stress for the active mono-slip. In all numerical analyses, we take $\xi = 10^{-6}m$, $\bar{\xi} = \xi b\rho_s = 2.5 \times 10^{-16} \times \rho_s$. Figure 3 shows the evolution of $Y(\bar{x}_2)$ for $\varphi = 30^0$, where $\bar{x}_2 = x_2 b\rho_s$.
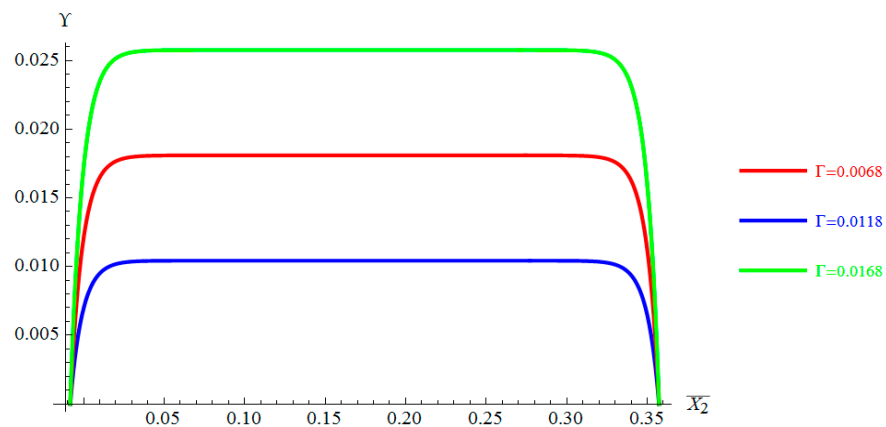
Figure 3. The evolution of plastic distortion (Y).

2.3.2. Non-Zero Energy Dissipation Case

Dislocation appears in crystals to reduce their energy. Energy dissipation analysis is more accurate than any other method to define the material features in the plastic phase. The displacement associated with reversible-to-irreversible reactions of the materials is commonly linked to the accumulation of continuum dislocations. The methods can be implemented to analyze the hysteresis energy triggered by the inclusions that create resistance in the unit cell. If the dislocation motion resistance cannot be avoided, the irreversible deformation advances as long as the yield condition is satisfied, that is, $\aleph = K$ [37]. The evolution of dislocation in MDCS can also be highly sensitive to the interaction between fibers and the matrix interface. If $|\aleph| < K$, then Y is fixed, the DOD is assumed to be constant, and the unit cell is reversibly distorted. Analyzing the variational derivative of Equation (21) yields the condition. The first case considered is $\varphi < \pi/4$.

$$\left| -Y \sin^2 2\varphi + \kappa Y \sin^2 2\varphi - \cos^2 2\varphi Y^{ave} + kY^{ave} \sin^2 2\varphi + kY_{,22} \sin^2 \varphi \left(b^2 \rho_s^2 \right)^{-1} + \Gamma \cos 2\varphi \right| = K/G_{12} \cos 2\varphi \quad (37)$$

The distribution of dislocation also leads to an escalation in entropy related to distortion. A strain energy state limits individual dislocation, which absorbs some of the plastic flow as the DOD increases [19,32]. According to Γ, the definite time function can be used to estimate $Y(t, x_2)$. The key is to determine the distortion as a function of time and x_2 in its evolution state, provided $Y(0, x_2) = 0$ and $\varphi < \pi/4$. Since the irreversible distortion, Y, is primarily zero, we observe from (38) that $Y = 0$ if, and only if, $\Gamma < \Gamma_{cr}$. Therefore, the yield stress condition for small $Y(t, x)$ and $\Gamma < \Gamma_{cr}$ becomes

$$- Y \sin^2 2\varphi + \kappa Y \sin^2 2\varphi - \cos^2 2\varphi Y^{ave} + kY^{ave} \sin^2 2\varphi + kY'' \sin^2 \varphi + \Gamma \cos 2\varphi = \Gamma_{cr} \cos 2\varphi \quad (38)$$

The deviation of $\Gamma(t)$ from the critical shear streamline (38) is introduced to obtain $\Gamma_f = \Gamma - \Gamma_{cr} \Rightarrow \Gamma = \Gamma_f + \Gamma_{cr}$ and $\Gamma_f = Y/Y_1$:

$$- Y \sin^2 2\varphi + \kappa Y \sin^2 2\varphi - \cos^2 2\varphi Y^{ave} = -kY^{ave} \sin^2 2\varphi - kY'' \sin^2 \varphi - \Gamma_f \cos 2\varphi \quad (39)$$

The analogous problem of dissipated energy in the constrained shear resistance suggests that the result of Equation (37) should be symmetric. Hence, $Y_1(x_2) = Y_1(\xi - x_2)$ *for* $x_2 \in (\xi/2, \xi)$. The function $Y_1(x_2)$ can be obtained from Equation (38). Similarly, we can use the boundary condition from Equation (33a). In the first case, the boundary region is far from the dislocations because of the stated displacement. In the next case, the plastic distortion is guided by continuity and symmetry. Based on this, Y_1 is evaluated as

$$Y_1 = Y_{1p}(1 - \cos h(\eta x_2) * (1 + Tanh(\eta \xi/2) * Tanh(\eta x_2)), 0 \leq x_2 \leq \xi/2 \quad (40a)$$

$$Y_{1p} = \left(\cos 2\varphi - Y_1^{ave}\left(\cos^2 2\varphi + \kappa\sin^2 2\varphi\right)\right) * \left[\sin^2 2\varphi - \kappa\sin^2 2\varphi\right]^{-1} \tag{40b}$$

$$\eta = \left(4(1-\kappa)k^{-1}\cos^2 \varphi\right)^{1/2} \tag{40c}$$

The average Y_1 is obtained as follows:

$$Y_1^{ave} = \left(\cos 2\varphi(\eta\xi - 2\text{Tanh}(\eta\xi/2))\right) * \left[\sin^2 2\varphi(\eta\xi) - \kappa(\eta\xi)\sin^2 2\varphi + \left(\cos^2 2\varphi + \kappa\sin^2 2\varphi\right)(\eta\xi - 2\text{Tanh}(\eta\xi/2))\right]^{-1} \tag{41}$$

In this part, we used the following numerical values for the simulation: $\xi = 1$ μm, so $\overline{\xi} = \xi b\rho_s = 2.5 \times 10^{-16} \times \rho_s$. Figure 4 depicts the evolution of $Y(\overline{x}_2)$ for $\varphi = 30^0$, where $\overline{x}_2 = x_2 b\rho_s$.
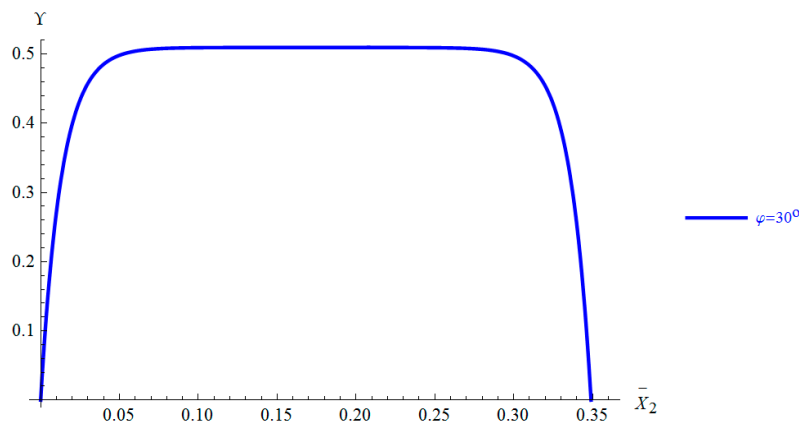
Figure 4. Evolution of plastic distortion (Y) in the energy dissipation case.

3. Numerical Expression and Discussion

As illustrated in this paper, in the unit cell of the composite material model, the continuum dislocation is mostly formed by complex variables of different parameters, for instance, the dislocation evolution, the material characteristic length l, and the behavior of the fiber/particle and the matrix. Therefore, it becomes a practical challenge to determine the equilibrium location of the dislocations. In this research, only edge dislocations in an active mono-slip system were considered. The slip plane direction is assumed to be in the x_2-direction, and the slip is taken to be in the x_1-direction.

When UCs are subjected to simple shear, there should be a dislocation in the veins of the matrix. During this process, the dislocation is trapped by the inclusion, and the number of dislocation densities increases, i.e., it results in hardening. The shear stress due to dislocation is termed micro shear stress, and the shear stress at the hardening point is referred to as critical shear stress. The equilibrium equation from this analysis is given as follows:

$$\tau_{cr} - \tau - \tau_{microstress} = 0 \tag{42}$$

From the free energy formula $\Theta\left(\varepsilon_{ij}^e, \alpha_{ij}\right)$, we can find the standard stress tensor σ_{ij} by using the thermodynamical approach:

$$\sigma_{ij} = \partial\Theta/\partial\varepsilon_{ij}^e = \tau \tag{43}$$

The micro stress τ_m is evaluated as follows:

$$\tau_m = e_{ijk}m_i\varsigma_{ij}s_j \tag{44}$$

where ς_{ij} is the distortion stress tensor. The distortion stress tensor is also calculated:

$$\varsigma_{ij} = \partial\Theta/\partial\alpha_{ij} \tag{45}$$

According to the law of thermodynamics, $\sum_{\kappa} \tau_{cr} Y \geq 0$ is constant per the inequality; it is also independent of the rate. We formulate the analytical equation as shown below:

$$\tau_{cr} = \chi \, sign Y \tag{46}$$

where $\chi > 0$ is the resistance of the slip represented by the formula shown in Equation (47):

$$\chi = hY \tag{47}$$

By using Equations (42)–(44), the standard shear stress is formulated:

$$\sigma_{12} = \frac{1}{2} G_{12}(u_{1,2} - Ys_1 m_2 - Ys_2 m_1) \tag{48}$$

We validated the method defined in the aforementioned parts by accounting for the BC formulations demonstrated in Figure 2. The material is assumed to be composed of a double episodic array of UCs with a width of $2w$ and height of 2ξ as shown in Figure 5 The UC can be defined in a state of typical shear distortion by setting kinematic BCs. Periodic boundaries are necessary along the lateral sides $x_1 = \pm w$. The term τ_{ave} (average shear stress) is required to withstand the distortions calculated from the shear field σ_{12} of the overall stress σ.

$$\tau_{ave} = \frac{1}{2w} \langle \sigma_{12}(\pm x_1, \pm \xi) \rangle_{(-w,w)} \tag{49}$$
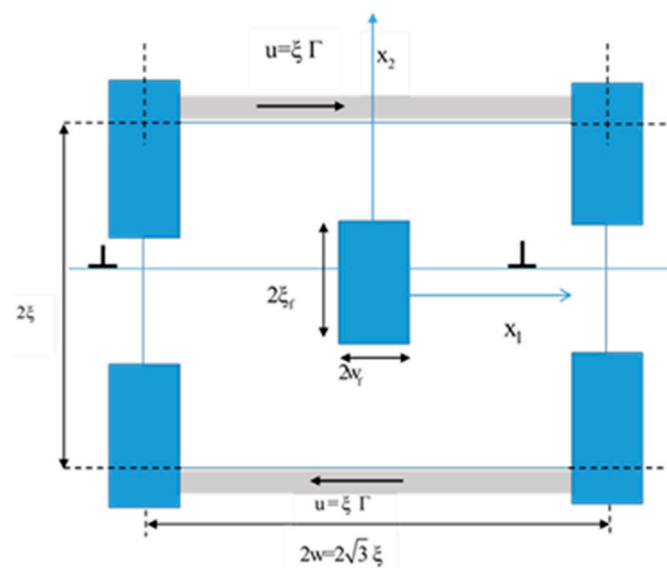
Figure 5. Unit cell of composite material with a periodic array of elastic particles.

The magnitude b denotes the Burgers vector of the overall dislocations in the unit cell, which has a value of $b = 2.5 \times 10^{-10} m$. In addition, two dislocations with contrasting b annihilate each other when they are dependent on material characteristic length; the critical annihilation length l_e is equal to $l_e = 6b$. All inclusions should have an identical value, which is equal to $\tau_{obs} = 5.7 \times 10^{-3} G_{12}$, where G_{12} denotes the elastic modulus of the shear. In the critical length, the stress created by shear distortion on the inclusion can be balanced by the dislocations generated in the slip plane. In the critical length, the value of K = 0.000115. The stress created due to dislocation nucleation corresponds to a nucleation length of $l_{nuc} = 125b$. The height ($\xi/2$) of the UCs is based on the material characteristic length (l), which equals 4000b. The influence of inclusion size is analyzed by changing the ratio ξ/l [43].

The parameter of the material represented by a metal matrix, specifically, an aluminum matrix, can be used for the overall numerical analysis, as described by different researchers [18]. The other isotropic material constants are E = 62.78 GPa and v = 0.33, where "E" and "v" denote Young's modulus and Poisson's ratio, respectively.

Figure 6 shows the total stress caused by shear deformation versus the recommended shear strain for the two categories of materials (materials I and II) in the unit cell, represented by $\xi = \ell$. The outcomes of discrete dislocations should also be included. For material II, the result of the continuum formulation of the dislocation value is similar to that obtained using the discrete formulation. Material I undergoes a yielding stage through the softening of the strain, while material II displays an approximately direct influence on the stress hardening.
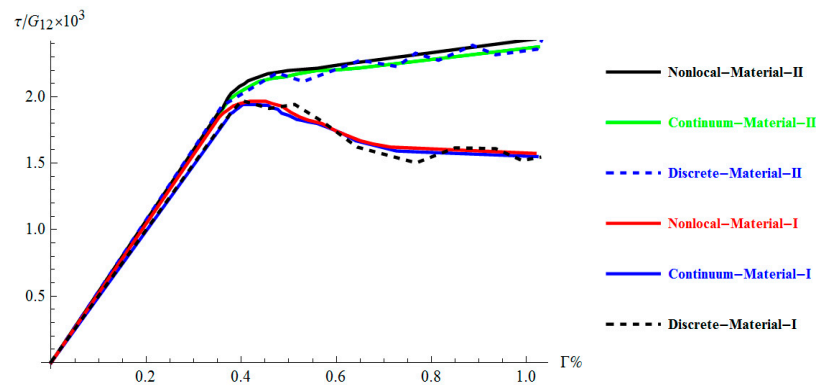
Figure 6. Comparison of shear stress and shear strain ($\tau - \Gamma$) for materials I and II.

In Figure 7, material II is characterized by a notably small size effect with stronger behavior. However, material I particles are larger size than those of material II, but it is not stronger. To measure the capability of the current continuum dislocation theory and enhance the size influence, we repeated the calculations for smaller $\xi = \ell/2$ and larger $\xi = 2\ell$ particle sizes, departing from the zone of the fractional constant. For material I, the two results are similar, while material II shows the predicted relationship. The logical conclusion from Figure 7 is that the rate of hardening and the strength of material flow increase as particle size decreases. Furthermore, the general hardness for all sizes of material particles can be directly connected to the strain.
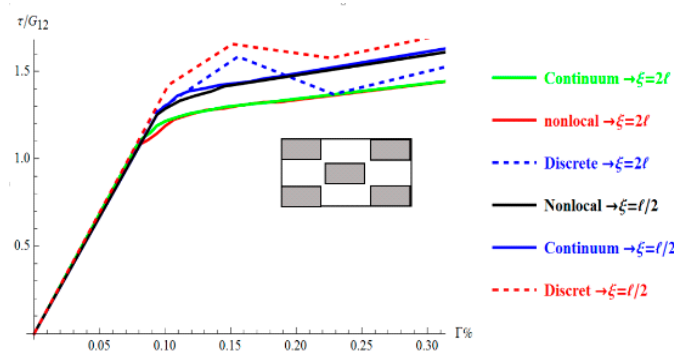
Figure 7. Stress–strain curve for material II.

The existence of GNDs in the unit cell was excluded to validate the changes in hardening, even though the volume fraction of the fiber part can be the same [28,29]. In the contemporary continuum dislocation concept, for identical materials, the values can be differentiated among diverse categories of dislocation distributions. However, it causes variance in the hardening conditions. Figure 8 indicates that the gradual development of the overall density of the dislocation in the deformed area is controlled by the length of the

material l in the unit cell. Generally, the increased accumulation of the dislocation density should occur before the direct strain is created, depending on the size of the particles. The density of dislocation increases as the particle size decreases, which is related to the dislocation effect on the discrete form.
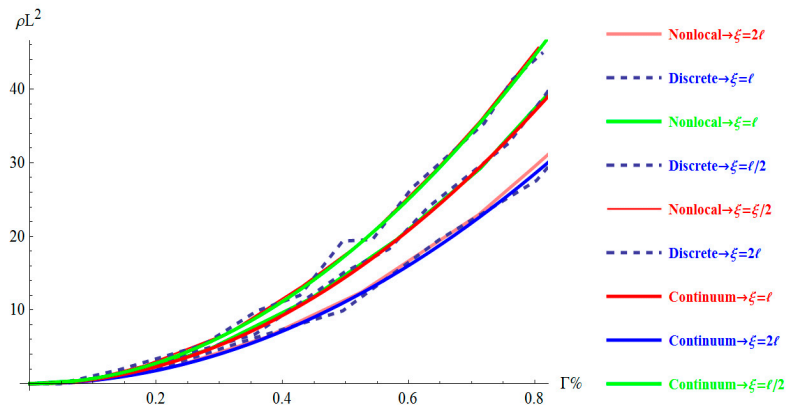
Figure 8. Overall dislocation density ρ evolution for zero energy dissipation compared with discrete and nonlocal distortion in material II.

The distributions of shear strain represented in Figure 9 for the two values of deformation indicate that a slight boundary plane can improve the active mono-slip system. For the continuum dislocation principle, the active mono-slip system through the distribution of shear strain in the continuum dislocation model is independent of $x_2 \varepsilon_{12}^{ave}(x_2) = \varepsilon_{12}(x_2)$. The distribution of strain is indicated in Figure 9 for both $\xi = \ell/2$ and $\xi = 2\ell$. The plot shows that it has a very slight size dependency and identical arrangement to that of the ε_{12}^{ave} distribution of [44]. Active one-slip system modeling was performed with $H_0 = 2\tau_{ref}$, and the outcomes did not qualitatively change from those indicated in Figure 9.
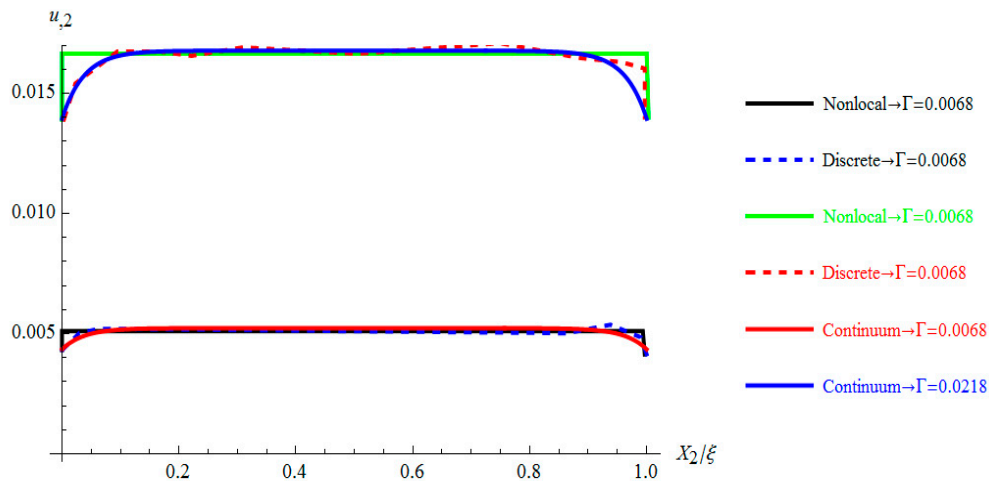
Figure 9. Shear strain profiles at two values of overall shear strain for a single slip compared with discrete and nonlocal distortion in material II.

4. Conclusions

In this paper, continuum dislocation theory is applied to analyze the plasticity theory of metal matrix composites in UCs. The theory is based on the energy characteristics of dislocations combined with typical small-strain continuum dislocation kinematics. Derivations of the continuum dislocation components, including slip formulation, thermodynamic concepts, free energy determinations, threshold values, and the evolution of dislocation, are described. Dissipation and non-dissipation formulations are derived using the variational

method and solved by the energy minimization approach. The outcomes are verified by comparing the existing discrete and nonlocal dislocation results with the newly formulated continuum dislocation theory results of the same problem. Furthermore, the effects of the material parametric length in the continuum dislocation theory analysis are reasonable and consistent with the existing discrete and nonlocal dislocation prediction. This newly formulated theory also agrees with the discrete and nonlocal dislocation result for a similar geometry and size. The capability of the proposed approach is demonstrated using a homogenized composite with constituents that exhibit different mechanical behaviors. The proposed method is found to be capable of handling the elastoplastic phenomenon of composite material, and more advanced micromechanics models can be implemented using the described approach. In summary, single-slip continuum dislocation can be modeled with the reported method, which includes self-stress conditions. Finally, two types of material models (Materials I and II) can be incorporated into the proposed approach.

Conflicts of Interest: The author declare no conflict of interest.

References

1. Kasa, T.T. Consideration of interlaminar strain–energy continuity in composite plate analysis using improved higher order theory. *Trans. Can. Soc. Mech. Eng.* **2018**, *42*, 211–221. [CrossRef]
2. Kasa, T.T. Inter-Laminar Strain Energy Continuity in Orthotropic Face Sandwich and Composite Plate Analysis Using Improved Higher-Order Theory. 2018. Available online: https://yorkspace.library.yorku.ca/xmlui/bitstream/handle/10315/35381/CSME2018_paper_5.pdf?sequence=1&isAllowed=y (accessed on 15 April 2020).
3. Kasa, T.T. Lightweight sandwich and composite beam analysis using improved higher-order theory with respect to strain energy fidelity in ply-wise approach. *Aust. J. Mech. Eng.* **2020**, 1–11. [CrossRef]
4. Takele, K. Interfacial Strain Energy Continuity Assumption-Based Analysis of an Orthotropic-Skin Sandwich Plate Using a Refined Layer-by-Layer Theory. *Mech. Compos. Mater.* **2018**, *54*, 281–298. [CrossRef]
5. Acharya, A. A model of crystal plasticity based on the theory of continuously distributed dislocations. *J. Mech. Phys. Solids* **2001**, *49*, 761–784. [CrossRef]
6. Chou, T.-W. *Microstructural Design of Fiber Composites*; Cambridge University Press: Cambridge, UK; New york, NY, USA, 2005.
7. Acharya, A. Constitutive analysis of finite deformation field dislocation mechanics. *J. Mech. Phys. Solids* **2004**, *52*, 301–316. [CrossRef]
8. Gurtin, M.E. A gradient theory of single-crystal viscoplasticity that accounts for geometrically necessary dislocations. *J. Mech. Phys. Solids* **2002**, *50*, 5–32. [CrossRef]
9. Kochmann, D.M.; Hackl, K.; Le, K.C. A continuum-dislocation theory for modeling dislocation microstructures and size effects in crystal plastiticy. In Proceedings of the 7th EUROMECH Solid Mechanics Conference, Lisbon, Portugal, 7–11 September 2009.
10. Mughrabi, H. On the role of strain gradients and long-range internal stresses in the composite model of crystal plasticity. *Mater. Sci. Eng. A* **2001**, *317*, 171–180. [CrossRef]
11. Schulz, K.; Sudmanns, M.; Gumbsch, P. Dislocation-density based description of the deformation of a composite material. *Model. Simul. Mater. Sci. Eng.* **2017**, *25*, 064003. [CrossRef]
12. Kasa, T.T. Continuum Dislocations and Active Single-slip Assumption in Micro-Mechanical analysis of Matrix Dominated Composite Unit cell. In Proceedings of the Canadian Society for Mechanical Engineering International Congress 2020, Charlottetown, PE, Canada, 21–24 June 2020.
13. Kröner, E. Continuum theory of defects. In *Physics of Defects*; Les Houches, Session 35; North-Holland: Amsterdam, The Netherlands, 1980.
14. Aharoni, H.; Machon, T.; Kamien, R.D. Composite dislocations in smectic liquid crystals. *Phys. Rev. Lett.* **2017**, *118*, 257801. [CrossRef]
15. Salehinia, I.; Shao, S.; Wang, J.; Zbib, H. Interface structure and the inception of plasticity in Nb/NbC nanolayered composites. *Acta Mater.* **2015**, *86*, 331–340. [CrossRef]
16. Li, N.; Demkowicz, M.; Mara, N.; Wang, Y.; Misra, A. Hardening due to interfacial He bubbles in nanolayered composites. *Mater. Res. Lett.* **2016**, *4*, 75–82. [CrossRef]

17. Mastorakos, I.; Abdolrahim, N.; Zbib, H. Deformation mechanisms in composite nano-layered metallic and nanowire structures. *Int. J. Mech. Sci.* **2010**, *52*, 295–302. [CrossRef]

18. Acharya, A.; Bassani, J. Lattice incompatibility and a gradient theory of crystal plasticity. *J. Mech. Phys. Solids* **2000**, *48*, 1565–1595. [CrossRef]

19. Hutchinson, J.W. Plasticity at the micron scale. *Int. J. Solids Struct.* **2000**, *37*, 225–238. [CrossRef]

20. Hoagland, R.G.; Kurtz, R.J.; Henager, C., Jr. Slip resistance of interfaces and the strength of metallic multilayer composites. *Scr. Mater.* **2004**, *50*, 775–779. [CrossRef]

21. Selvam, J.D.R.; Dinaharan, I.; Philip, S.V.; Mashinini, P. Microstructure and mechanical characterization of in situ synthesized AA6061/(TiB2+ Al2O3) hybrid aluminum matrix composites. *J. Alloys Compd.* **2018**, *740*, 529–535. [CrossRef]

22. Fan, M.; Xiao, Z.; Luo, J. On the plastic zone correction of a Zener–Stroh crack interacting with a nearby inhomogeneity and an edge dislocation. *Acta Mech.* **2015**, *226*, 4173–4188. [CrossRef]

23. Eringen, A.C. Nonlocal polar elastic continua. *Int. J. Eng. Sci.* **1972**, *10*, 1–16. [CrossRef]

24. Eringen, A.C.; Wegner, J. Nonlocal continuum field theories. *Appl. Mech. Rev.* **2003**, *56*, B20–B22. [CrossRef]

25. Chen, Y.S. Continuum Theory of Self-Similar Dislocation Cellular Structures. Ph.D. Thesis, Cornell Univerisity, Ithaca, NY, USA, 2012.

26. Zhang, C.; Li, N.; Wang, W.; Binienda, W.K.; Fang, H. Progressive damage simulation of triaxially braided composite using a 3D meso-scale finite element model. *Compos. Struct.* **2015**, *125*, 104–116. [CrossRef]

27. Fan, M.; Xiao, Z.; Luo, J. Application of cohesive zone model in crack propagation analysis in multiphase composite materials. *Mech. Adv. Mater. Struct.* **2017**, *24*, 1109–1115. [CrossRef]

28. Cleveringa, H.; Van Der Giessen, E.; Needleman, A. Comparison of discrete dislocation and continuum plasticity predictions for a composite material. *Acta Mater.* **1997**, *45*, 3163–3179. [CrossRef]

29. Cleveringa, H.; Van der Giessen, E.; Needleman, A. A discrete dislocation analysis of bending. *Int. J. Plast.* **1999**, *15*, 837–868. [CrossRef]

30. Ghosh, S.; Lee, K.; Raghavan, P. A multi-level computational model for multi-scale damage analysis in composite and porous materials. *Int. J. Solids Struct.* **2001**, *38*, 2335–2385. [CrossRef]

31. Greer, J.R.; De Hosson, J.T.M. Plasticity in small-sized metallic systems: Intrinsic versus extrinsic size effect. *Prog. Mater. Sci.* **2011**, *56*, 654–724. [CrossRef]

32. Nye, J. Some geometrical relations in dislocated crystals. *Acta Metall.* **1953**, *1*, 153–162. [CrossRef]

33. Berdichevsky, V.L. Continuum theory of dislocations revisited. *Contin. Mech. Thermodyn.* **2006**, *18*, 195. [CrossRef]

34. Fan, M.; Yi, D.; Xiao, Z. Fracture behavior investigation for a pileup of edge dislocations interacting with a nanoscale inhomogeneity with interface effects. *Int. J. Damage Mech.* **2015**, *24*, 891–914. [CrossRef]

35. Koslowski, M.; Cuitino, A.M.; Ortiz, M. A phase-field theory of dislocation dynamics, strain hardening and hysteresis in ductile single crystals. *J. Mech. Phys. Solids* **2002**, *50*, 2597–2635. [CrossRef]

36. Schulz, K.; Sandfeld, S.; Gumbsch, P. A Three-dimensional Continuum Theory of Dislocation Plasticity-Modelling and Application to a Composite. *PAMM* **2011**, *11*, 437–438. [CrossRef]

37. Berdichevsky, V.; Le, K. Dislocation nucleation and work hardening in anti-plane constrained shear. *Contin. Mech. Thermodyn.* **2007**, *18*, 455–467. [CrossRef]

38. Hutchinson, J.; Fleck, N. Strain gradient plasticity. *Adv. Appl. Mech.* **1997**, *33*, 295–361.

39. Shu, J.; Fleck, N.; Van der Giessen, E.; Needleman, A. Boundary layers in constrained plastic flow: Comparison of nonlocal and discrete dislocation plasticity. *J. Mech. Phys. Solids* **2001**, *49*, 1361–1395. [CrossRef]

40. Fleck, N.; Muller, G.; Ashby, M.F.; Hutchinson, J.W. Strain gradient plasticity: Theory and experiment. *Acta Metall. Mater.* **1994**, *42*, 475–487. [CrossRef]

41. Berdichevsky, V. On thermodynamics of crystal plasticity. *Scr. Mater.* **2006**, *54*, 711–716. [CrossRef]

42. Weygand, D.; Friedman, L.; Van der Giessen, E.; Needleman, A. Aspects of boundary-value problem solutions with three-dimensional dislocation dynamics. *Model. Simul. Mater. Sci. Eng.* **2002**, *10*, 437. [CrossRef]

43. Bassani, J.; Needleman, A.; Van der Giessen, E. Plastic flow in a composite: A comparison of nonlocal continuum and discrete dislocation predictions. *Int. J. Solids Struct.* **2001**, *38*, 833–853. [CrossRef]

44. Bittencourt, E.; Needleman, A.; Gurtin, M.E.; Van der Giessen, E. A comparison of nonlocal continuum and discrete dislocation plasticity predictions. *J. Mech. Phys. Solids* **2003**, *51*, 281–310. [CrossRef]